CBET lolol

(Hopefully soon to be Dr.) Philip W. X. Moloney

IMPERIAL

June 2024

Submitted in partial fulfilment of the requirements for the degree of
Doctor of Philosophy of Imperial College London

Department of Physics
Imperial College London
Prince Consort Road
London SW7 2AZ

List of Acronyms

Rad-MHD Radiative-Magnetohydrodynamics

Rad-Hydro Radiative-Hydrodynamics

HEDP High Energy Density Physics

LPIs Laser-Plasma Instabilities

CBET Cross-Beam Energy Transfer

ICF Inertial Confinement Fusion

PiC Particle in Cell

GO Geometric Optics

IB Inverse-Bremsstrahlung

SBS Stimulated Brillouin Scattering

PCGO Paraxial Complex Geometric Optics

IRT Inverse Ray Tracing

FRT Forward Ray Tracing

LLE Laboratory for Laser Energetics

LLNL Lawrence Livermore National Laboratory

CEA Commissariat à l'Énergie Atomique et aux Energies Alternatives

IAW Ion Acoustic Wave

OpenMP Open Multi-Processing

MPI Message Parsing Interface

1 Solas, A 3-D Laser Ray Trace and Cross-Beam Energy Transfer Model

This chapter will describe the Solas code, a 3-D Laser ray tracing module implemented in the Radiative-Magnetohydrodynamics (Rad-MHD) code Chimera. The chapter begins with a discussion of why ray tracing is frequently used to model 'long-pulse' lasers for High Energy Density Physics (HEDP) experiments and why the standard framework is inadequate to model Laser-Plasma Instabilities (LPIs). It will then go on to describe the ray-trajectory solver, electric-field reconstruction and Cross-Beam Energy Transfer (CBET) components of the model in detail. Discussion of the validity of the model components will be included. The numerical methods will also be presented alongside an extensive set validation problems to verify the implementation.

1.1 Ray Tracing for Hydrodynamic Simulations of Fusion Plasmas

Nanosecond length ('long-pulse') lasers are often used as an external energy source in the field of HEDP, for example in laboratory-astrophysics experiments [1–3], equation of state studies [4, 5] or Inertial Confinement Fusion (ICF) implosions [6–8]. Experimental design and analysis for these experiments must often be supported with fluid Rad-MHD simulations. The laser must therefore be described in these codes by a theoretical framework that is both valid to the problem and computationally tractable. The physical processes by which lasers interact with plasma is a result of microscopic couplings between the laser field and particles or plasma waves. The detailed microphysics of these interactions are often studied using Particle in Cell (PiC) codes [9] or wave-based solvers [10], typically for scales and durations of tens of micrometres and hundreds of picoseconds. Coupling these tools directly to multidimensional hydrodynamic simulations, which are often used for millimetre and nanosecond scales, would usually be computationally intractable.

The Geometric Optics (GO) assumptions are often widely applicable for HEDP laser-plasma interactions (validity discussed in detail for ICF plasmas in section 1.5.8) and therefore ray-tracing offers a computationally tractable approach to modelling lasers in these experiments. By assuming static hydrodynamic profiles (which is normally valid for the propagation time of light through the computational domain) a laser beam can be discretized into a bundle of rays and the ray equations can then be integrated along their path to solve for the trajectory of the light, assuming that refraction dominates over diffraction. A discrete amount of power can also be given to each ray. If there is a suitable model for the power-absorption rate, this can also be integrated along the ray to provide an energy source for the plasma. In many laser-driven HEDP experiments, frequency-doubled or -tripled lasers and long scale-length plasmas mean that Inverse-Bremsstrahlung (IB) is the dominant deposition process [11, 12]. There are well established models for IB that are suitable for implementation in ray-tracing codes, because they only require knowledge of the local plasma conditions, which are easily accessible via interpolation from the hydrodynamic grid to rays [13, 14]. The combination of the ray equations and IB deposition therefore is the basis for the vast majority of laser-modules coupled to hydrodynamic codes.

In laser-driven ICF experiments however, another class of interaction, LPIs are vitally important to the energetics of the implosion. For example CBET leads to a zeroth-order correction to the energy deposited in direct-drive experiments at the OMEGA laser facility, reducing coupled power late in the implosion to $\sim 50\%$ [15]. LPIs cannot be included in the simple framework described above because they are non-linear[1] and reduced theoretical models of the interaction rely on knowledge of the electric field or intensity of the light [16]. Implementation in a tracing code therefore necessitates a method by which the separate light waves can 'talk' to each other. For example, the CBET code described in this chapter stores information for separate components of laser beams on a common grid which can then interact via the 'pump-depletion iterations', described in section 1.5.7. Additionally, the knowledge of electric field or intensity is problematic because this is not an attribute which standard GO rays posses. Heuristically, rays have an associated power, so an area is required to obtain an intensity. The evolution of a portion of the beam front's area is governed by a first order expansion of the Helmholtz equation, rather than the zeroth order expansion which is most commonly used in ray-tracing packages for hydrodynamic codes [17]. The first order expansion introduces an equation for the ray amplitude which can be solved in a variety of ways and used to obtain the electric field of the light. Section 1.4 describes the approach taken to solving for the amplitude of the rays in Solas, which is to track the area of a triangle[2] of rays around a standard GO ray.

For direct-drive ICF simulations, it is also desirable to have a 3D ray trace, where rays travel and refract in 3 dimensions. In some computational direct-drive studies, particularly in 1D hydrodynamic simulations, simplified laser models are employed in which rays travel radially toward the target [18]. This simplification is can lead to significant deviations from reality, as it neglects any refractive losses, which become increasingly significant late in the implosion as the target converges. Assuming that rays travel radially inward also leads to deposition occurring closer to the critical surface compared to a true 3D ray trace, leading to an overestimation of the drive. The growth of LPIs also depends on vector summations of light and plasma wavevectors, so a 3D

[1]Non-linear in this context means that the interaction involves the interaction of multiple light and plasma waves.

[2]For a 2D ray trace, a pair of rays is used rather than a triangle.

ray trace is necessary when modelling these effects. Predictive direct-drive simulations therefore necessitate a fully 3D ray-trace, even when coupled to just 1D hydrodynamics.

1.2 Existing Cross-Beam Energy Transfer Models

There are a variety of existing computational tools used to model CBET for ICF conditions, which are used to study the interaction from first principles, reduced models to investigate the effect of CBET when coupled to hydrodynamics or validation tools to test the implementation of these reduced models. A non-exhaustive list will be presented here of existing codes, provided mainly as context for the work presented in this chapter.

1.2.1 Ray Based Models

The most common tool to study the coupling of CBET effects into hydrodynamics are reduced ray-based models which use the linear gain theory of Stimulated Brillouin Scattering (SBS), outlined in section**??**. There are a variety of different codes used to simulate this. The main difference between the models is the way that the electric field or intensity of the laser light is obtained.

Inverse Ray Tracing (IRT) This is an approach, implemented within the IFRIIT code, that creates a mapping between points on an initial beam front and arbitrary locations within the plasma [19, 20]. This is in contrast to Forward Ray Tracing (FRT), which is used in the other ray-based approaches listed below, where discrete points on the beam front are integrated forward to discrete points within the plasma. IRT is a very efficient approach for convex, approximately spherically symmetric plasma profiles, it can not deal well with beams that have multiple caustics[3], where the FRT approach is better suited. IFRIIT has been coupled to the 3-D Radiative-Hydrodynamics (Rad-Hydro) code, ASTER from Laboratory for Laser Energetics (LLE), and prior to the development of SOLAS, ASTER-IFRIIT was the only code combination capable of conducting 3-D direct-drive simulations with in-line CBET [15].

Ray Statistics Approach The LASNEX [21], TROLL [22] and DRACO codes [23], developed at Lawrence Livermore National Laboratory (LLNL), Commissariat à l'Énergie Atomique et aux Energies Alternatives (CEA) and LLE respectively, implement field-reconstruction methods which depend heavily on having many rays per computational cell. LASNEX and TROLL, used mainly for indirect-drive hohlraum simulations, obtains the intensity of light by first propagating rays through the mesh and obtaining the deposited power in each grid cell. The intensity is then obtained from the power in each cell using electromagnetic energy conservation. Obtaining the intensity from deposition means that the field cannot be reconstructed in vacuum regions where no deposition occurs.

[3]Caustics are defined and discussed in detail in section 1.4.1.

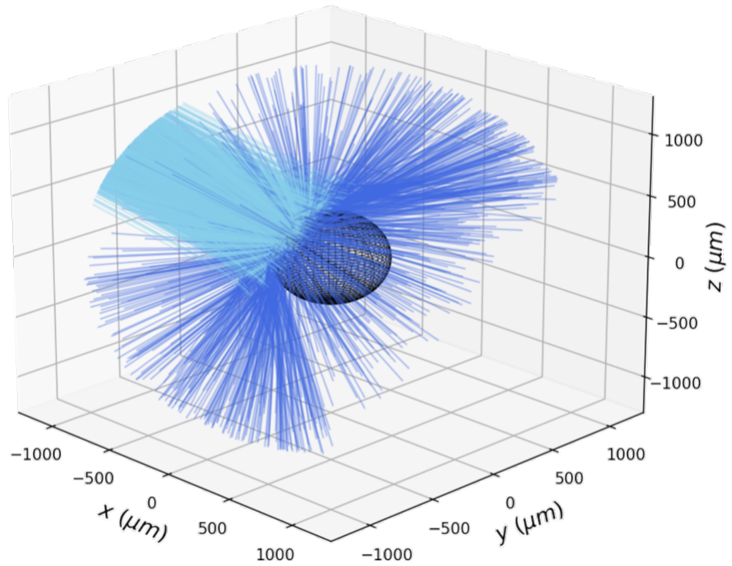

Figure 1.1: 3D ray trajectories through a spherically symmetric, OMEGA direct-drive scale density profile. The incident rays are plotted in cyan and the reflected rays, which spread out over a very large solid angle, are plotted in dark blue. The critical density is represented by the black mesh.

DRACO uses a similar approach, but the intensity is estimated by multiplying the ray power by the path length in a cell divided by the cell volume, which gives a dimensional estimate for the intensity. Both of these approaches require a large number of rays-per cell to accurately obtain the intensity, $\mathcal{O}(100)$ [24]. For direct-drive simulations this is extremely computationally expensive, because backscatter CBET dominates over sidescatter, therefore the reflected field of each beam must be resolved, and each beam spreads out over a large solid angle after reflecting off a convex density profile, as is demonstrated in figure 1.1. This means that orders of magnitude more rays are required than for approaches which can accurately obtain the field from a single ray per cell.

Another drawback of both of these approaches is that caustics of beams (regions where the amplitude of rays diverge) are not identifiable, and therefore fields cannot be capped to physically accurate, diffraction-limited values. If a significant amount of CBET occurs at caustics, such as in direct-drive ICF, then erroneous global multipliers to CBET gains must be applied which are effectively free parameters that must be tuned to obtain a pre-known reduction in absorbed energy. This means that it is difficult to trust this approach for predictive direct-drive simulations.

Paraxial Complex Geometric Optics (PCGO) In this approach, each ray has an associated Gaussian intensity profile, the width of which is integrated along the ray trajectory [17, 25**?**]. A single ray can be used per cell as each ray can have an intensity which is interpolated to the mesh, but the reconstructed field at caustics is not accurate and the width evolution is only valid for a short propagation distance. This approach was coupled to the CHIC 2 dimensional hydrodynamics code, but is difficult to extend to

3D as the implementation relied on interacting only rays whose centroids crossed, which does not generically occur in 3D for non-coplanar rays [26].

Neighbouring Rays The BeamCrosser code obtains an area for each ray by co-tracing a triangle of neighbouring rays around it that can be converted into a ray amplitude and therefore electric field from electromagnetic energy conservation [27]. Integrating the amplitude along the ray trajectory means that the caustics can be identified and therefore fields in those regions capped to diffraction limited values [28]. Each ray also has an individual field value, and it is therefore less dependent on ray-per-cell statistics than geometric models, such as that used in the Draco code described above [29]. Section 1.4 describes the implementation of this approach into the Chimera 3D Rad-MHD code, which had not previously been used coupled to hydrodynamics in multidimensional simulations.

1.2.2 Wave Solvers

Solving Maxwell's equations with coupling to a plasma background is a useful tool for the study of LPIs. The main code used in the ICF community that uses this approach is Lpse, which propagates light waves through a prescribed, spatially varying density, temperature and velocity profile in 1D→3D [10, 30]. It then solves the nonlinear coupling of electromagnetic waves by allowing first order plasma perturbations (obtained from the ponderomotive beat pattern between light), which then feed back into the wave propagation. The perturbative approach means that Lpse is limited to linear problems and the temporal and spatial resolution required to resolve the beat frequency mean that coupling to multidimensional Rad-Hydro simulations is not feasible. However, it is an extremely useful tool to validate implementation of CBET models, especially in situations like scattering at laser caustics, such as the test case presented in section 1.5.10.2. It can also been used for many other important studies, such as the mitigation of LPIs via laser bandwidth and the effect of beam smoothing techniques on the growth rate of LPIs [31].

1.2.3 PiC Codes

Both Ray based codes and Lpse are ill-suited to the study of LPIs in the non-linear regime, where the laser intensity becomes sufficiently large that the ponderomotive imprint on the plasma can no longer be treated perturbatively. Understanding this growth and saturation of LPIs in this regime is particularly important for ICF schemes with high peak intensities, such as during the ignitor spike in shock ignition pulses [32]. Often kinetic effects such as ion-trapping become important in non-linear saturation, where ion are trapped and then accelerated in the CBET induced Ion Acoustic Wave (IAW), leading to changes in the IAW phase velocity and therefore a loss of resonance [9]. PiC codes are therefore well suited to model this kinetic saturation, albeit over short timescales and in simulations that are not truly representative of direct-drive conditions, due to

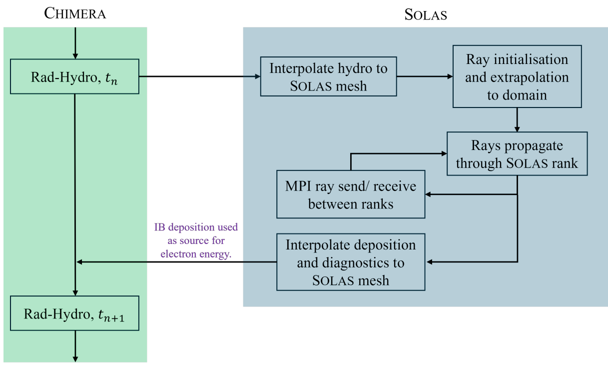

Figure 1.2: A flowchart illustrating the basic interfacing between CHIMERA and SOLAS. The interpolation steps refer simultaneously to the re-domain balancing and cell combination procedures described in section 1.3.1

computational expense [33]. Kinetic modelling of CBET has demonstrated that the growth of LPIs can be a much more complex, time-dependent problem than is assumed by the linear-models used in ray-based codes, leading to larger net energy transfers [34].

1.3 SOLAS 3-D Laser Ray Trace

This section will describe how the ray equations, derived from the Helmholtz equation in section **??** are solved in the SOLAS module for the CHIMERA Rad-MHD code. Details of the mesh used for spherical simulations and load balancing options shall be provided as well as validation problems.

A simple flowchart for the basic SOLAS operational loop and the interfacing with CHIMERA is shown in figure 1.2. The interpolation, initialization and propagation steps will be outlined in sections 1.3.1, 1.3.2, 1.3.3 respectively.

1.3.1 SOLAS Mesh Structure

The mesh used for hydrodynamic calculations is often not well suited for ray tracing calculations.

HERE TALK GENERICALLY ABOUT SCALE LENGTHS ETC., OVERCRITICAL CELLS

1.3.1.1 Re-Domain Balance for Radial Geometries

Rad-MHD codes often employ a domain balanced approach to parallelization[4], where each computational rank solves a portion of the entire spatial domain each discrete timestep. Additional ‘ghost-cells’ are stored in the subdomains and used to calculate gradients on the boundaries between ranks, which are updated with inter-rank communications each timestep. The hydrodynamic grid for CHIMERA is Eulerian, with options for Cartesian, cylindrical or spherical-polar grids.

[4]This includes the CHIMERA code for which SOLAS has been developed.

The optimal domain balancing minimises communication between ranks, which leads to cubic[5] subdomains. If computing a laser raytrace through this domain however for a typical direct-drive calculation however, initially rays travel approximately radially and therefore regularly encounter processor boundaries where they must be transferred between ranks. A more optimal domain decomposition for the raytrace minimises radial splitting to avoid excessive passing of rays. When required for spherical and cylindrical simulations, Solas therefore takes the hdyrodynamic variables on the Chimera grid and re-domain balances the grid for the raytrace, such that the splitting does not occur in the radial coordinate, as is shown in figure MAKE FIGURE HERE!!!

Note that a domain balanced, Message Parsing Interface (MPI) communication approach has been employed for the Solas grid and ray transfer. An alternative approach to parallelization of the module would be to use the Open Multi-Processing (OpenMP) package, where processors share memory across a computational node. In this approach, the entire laser grid would be stored once on the shared memory of the node and separate ranks would trace rays through the entire domain without the need for transfers. While this is certainly a preferable approach for a standard raytrace to the MPI procedure described above, including a model for CBET is more challenging with this approach. This is because CBET requires communication between beams and therefore large amounts of information must be stored on the grid, which can lead to large memory overheads. Therefore, using multiple computing nodes is often a necessity for 3D CBET calculations and OpenMP-MPI hybrid approaches are required which was deemed too significant an undertaking for the scope of the work presented in this thesis.

1.3.1.2 Semi-Structured Eulerian Grid with Combined Cells

Mention that also for 3D Eulerian spherical meshes near the poles, cell volumes go to zero. At a minimum to estimate laser quantities within a cell, the requirement for total number of rays is therefore dictated by the polar region. Equivalently for a given number of rays, noise will be much worse at the poles. Therefore, a novel 'semi-structured' grid was designed to circumvent this issue without giving up the advantages of an Eulerian grid (ease of implementation and interpolation between grids). Cells are combined in phi and theta to have the same dphi and dtheta as the equatorial cells on the grid, giving a roughly equal area on each raidla surface.

Also mention how cells are combined in r adaptively, which gives improved resolution in the vicinity of the caustic, where deposition, CBET and refraction are singificant. Note however that resolution is limited to the hydrodynamic resolution and the laser grid is not entirely separate. This does make interpolation between grids easier though.

1.3.2 Ray Initialisation

Give details on random sampling, uniform and invers-projection methods explaining their relative strengths and weaknesses.

[5]Cubic in number of cells, not necessarily in physical space for non-Cartesian geometries.

1.3.3 Equations of Rays and Adaptive Integration

The partial differential equations that are integrated along the trajectory of each ray are,

$$\begin{aligned}\frac{d\mathbf{x}}{d\tau} &= \mathbf{k} \\ \frac{d\mathbf{k}}{d\tau} &= \frac{1}{2}\nabla\varepsilon(\mathbf{x}) \\ \frac{d\varphi}{d\tau} &= \frac{\omega}{c}\varepsilon(\mathbf{x}) \\ \frac{d\omega}{d\tau} &= \frac{\omega}{2c}\frac{\partial\left(n_e/n_c\right)}{\partial t},\end{aligned} \tag{1.1}$$

Also mention here why I didn't use Kaiser solution (refraction from Snell was found to create unacceptable noise in the ray amplitude estimation). Somewhere mention that ray deposition is interpolated onto neighbouring cells using shape functions to reduce noise. Talk about how additional quantities are integrated along ray trajectory which are described in CBET section. However, the derivatives of these other things are assumed to be constant over a single laser step and therefore are not included in the adaptive integration.

Talk about how we use adaptive RK4 to integrate rays. Mention that adaptive solvers allow large steps in flat regions and accurately resolve the turning points.

1.3.3.1 Ray Solver Validation

Quadratic trough, cylindrical helix and blast wave tests

Quadratic trough Basic test of ray solver.

Cylindrical Helix Test of refraction in non Cartesian coordinates and also of refraction in directions without gridding.

Blast wave Test of inverse Bremmstrahlung absorption.

1.4 Ray Based Field Reconstruction and Ray Sheets

Say that we want to find the field to get CBET. For rays this means solving the transport equation to get ray amplitude and then using amplitude to get field. Talk about the concept of ray amplitude and how it can be related to an area of adjacent rays.

1.4.1 Amplitude Estimate from Neighbour Rays

Go into detail about how the area is obtained from neighbour rays. Talk about the concept of sheets and caustics as divergence of amplitude. Also talk about 'Interpolation' from rays to cells and vice versa.

1.4.2 Caustic Field Capping

Say that since amplitude diverges in the caustic region, necessary to cap it. In reality diffraction would limit the field in this region, but standard geometric optics rays can't model diffraction. Therefore typical approach which we follow is to limit the reconstructed field to a sensible, diffraciton-limited value.

1.4.2.1 Field Limiter Approach

Say that this is the approach used throughout the thesis apart from in some validation problems where it is labelled. Caps the field to the maximum of a Airy function (ray going up linear density profile).

1.4.2.2 Etalon Integral

This is an improvement which basically allows for deviations from linearity. This is not used normally, other than when cell size « wavelength, because it needs knowledge of the other sheet from the beam which is present in caustic region. Could be implemented using linear interpolation. However, typically we don't have sufficient angular resolution in combined cell grid (at least for 1D hydro) to reliably interpolate sheet to sheet via this grid. It is generally observed however that the field limiter approach is sufficient.

1.4.3 Field Reconstruction Validation

Using Russ' paper with lovely test comparisons to Lpse. Define the electron density profile here.

1.4.3.1 1D Reflected Beam

Just a simple test of field capping compared to an analytic problem, without refraction.

1.4.3.2 2D Reflected Beam

Same as above, but now for non-normally incident rays, accounting for refraction. Show test results in both Cartesian and Cylindrical.

1.5 Ray Based CBET Model

Explain that ray based CBET uses the linear gain discussed in theory section. Say that since this assumes homogineity, effectively applies to small ray steps, which is typically well satisfied. Also say that this homogeneity within a computational cell and nearest neighbour interpolation of field means that it is not necessary to adaptively integrate the CBET gain.

1.5.1 Power Change of Rays due to CBET

Describe how ray energy changes due to CBET from linear gain models (either fluid or kinetic). Say how when including with inv brem, the deposited power and CBET change must be got carefully (i.e. Marozas paper).

1.5.1.1 Fluid CBET Gain

Breifly discuss the fluid CBET gain and explain why it is easier to use for code validation.

1.5.1.2 Kinetic CBET Gain

Breifly discuss the kinetic CBET gain and why it is better for predictive simulations.

1.5.2 Dynamic memory structure for storing Fields and CBET Gains

Give the scaling of storing fields and gains for every beam. Say that therefore a dynamic memory structure is used which only stores the fields and gain in cells where they are present. Also state that although the ray trace module must be done in double to numerical errors (e.g. omega differences in resonance and difference between rays), gain is stored as a single which greatly reduces cost. Give an estimate for how much this reduces the overall memory requirements.

1.5.3 Doppler Shift of Frequency

Mention time dependant refractive index results in a frequency shift of light. This is small, however it is significant to include in CBET models as it can shift the resonance.

1.5.4 Caustic Gain Truncation

Say that because nearest neighbour interpolation of the fields is used, there exists unphyscial interaction regions where a cell has a field but ray hasn't passed through that portion of the cell. This problem becomes particularly bad at ray turning points, where a significant amount fo CBET occurs. Therefore a method called 'CGT' is used to effectively enhance the laser grid resolution in the vicnity of caustics. In cells where a ray from a specific sheet experience a caustic, the field entry for that sheet is divided geometrically, assuming that the caustic is locally a plane. If a ray from another sheet passes through the cell and is on the 'unlit' side of the caustic plane, it will not experience CBET gain. Ray steps are also limited to the caustic plane. Other codes have shown that this approach significantly improves energy conservation.

1.5.5 Coherent Caustic Correction and Caustic Region Identification

Say how the field reconstruction assumption works everywhere apart from at caustics, where it underestimates the field. Follow what Russ says in his paper about CC correction and how it significantly improves energy conservation.

1.5.5.1 Geometric Approach to identifying the caustic region

Other codes find caustic region by phase diff and phase interpolation. We can't interpolate due to resolution issues. Therefore implemented a new, geometric approach to finding the caustic region. Talk about how location of rays is stored for each sheet, partitioned by whether they are over or under the amplitude cap. If a cell has rays from both in a cell, then a plane is found between the two to split the cell into caustic and non-caustic. If a cell has only capped rays then the whole thing is caustic. When a ray from another beam passes through, CC mult is applied if in the caustic region.

1.5.6 Energy Conservation in Ray Based CBET Models

Talk about how energy is conserved away from caustics when converged.

1.5.7 Pump Depletion Iterations

Talk about why it is necessary to iterate the ray trace. Mention that it is possible to store ray locations and avoid performing ray trace all over again, but that approach is not taken due to memory limitations. Talk about convergence parameter. Mention necessity of damping for complicated, many beam simulations.

1.5.8 Model Assumptions, Applicability and Validity to ICF

Discuss the key assumptions of the CBET model and whether it is valid to use for LDD and LID.

1.5.9 Computational Efficency and Scaling

Talk about how the CBET model is quite expensive. Give the scaling laws from Russ' paper and explain how that means for many beams, CBET is bound to be the dominant cost in the simulation. Also say how it shows that memory is a big consideration for CBET models as the gains and fields must be stored.

1.5.10 CBET Validation

Using Russ' paper with lovely test comparisons to Lpse. Define the electron density profile here.

1.5.10.1 2D CBET Without Caustics

Just a simple test of field capping compared to an analytic problem, without refraction.

1.5.10.2 2D CBET With Caustics

Same as above, but now for non-normally incident rays, accounting for refraction. Show test results in both Cartesian and Cylindrical.

1.6 Coupling to Hydrodynamics and Example Use

Here present an entire explanation for the model working coupled to Hydrodynamics.

1.6.1 Power Deposition

Say that the deposited power is just added as an energy source to the electrons. If running in 1D or 2D, it is integrated over other directions first. Say that when starting from $t = 0$, often use a cold-start routine, which uniformly deposits power at the critical surface of a spherical capsule. This creates an under-dense small region in which the rays can refract and deposit energy. This is unsatisfactory for imprint simulations, where early time imprinting is important, but that is not considered for this thesis.

1.6.2 Time step limiter

Limit timstep based on the fractional electron energy change. Don't limit timestep in cells far from critical. This is usually the limitting timestep for 'cold start' simulations initially, until deposition begins to occur in hot cells.

1.6.3 Ray Trace Frequency

For many beam simulations, such as direct-drive simulations, the laser operator (especially with CBET) is typically one of the more expensive parts of the code. In the steady state of an implosion, the coronal plasma conditions don't significantly change on the global hydrodynamic timestep. Therefore the deposition also doesn't change much meaning that previously calculated Pdep can be stored and reapplied on subsequent timesteps. Especially for CBET simulations, this can reduce runtime by order of magnitude. Currently the ray trace is performed every timestep up until a pre-specified 'warm up' time has expired. Then the ray trace is performed at a pre-specified frequency by the user. Experimentation has found that for Omega scale simulations, increasing frequency of calculations doesn't significantly change the answer above ... .

Because LDD pulses often start with a low intensity and then ramp up, CBET gains are also often minimal until late in the implosion. Therefore field reconstruction and CBET iterations are only performed after a specified start time, normally when the hard-sphere intensity reaches about $1 \times 10^{14}\ Wcm^{-2}$. CBET iterations are then performed on the laser frequency.

An improved approach shall soon be implemented where laser iterations occur at dt_{laser} from section 1.6.2.

1.6.4 Computational Diagnostics

Say that a variety of diagnostics can be output. Qpower with and without CBET. Geometric intensity. Electric field (from single or all beams), optionally split into inbound and reflected components, both with and without CBET.

1.6.5 Example use on Omega Shot 89224

First briefly describe the shot, showing pulse shape and target.

1.6.5.1 1-D Rad-Hydro, 3-D Ray-Trace with CBET Simulation

Describe the simulation parameters used, e.g. cell resolution, flux limiter etc. Show the absorbed power vs time and effect of CBET. Show instantaneuos radial profiles. Show integrated parameter comparison to Lilac post-shot simulation. Describe the previous method of tuning, involving a 2D scan of flux limiter and power multipliers. Say how it's great that the $flim_e = 0.06 \rightarrow 0.15$ and CBET combination now gives a predictive capability for Omega shots.

1.6.5.2 3-D Post Process of Absorption Non-Uniformity

Mention how the model can also be used as a postprocess. Chimera can restart from 1-D data into spherically symmetric 3-D profiles. Ray Trace and CBET can then be performed through these profiles to understand the absorption non-uniformity present due to CBET. Note that comparison of 1-D and 3-D simulations shows that thermal conduction does a good job of smoothing angular deviations in coronal plasma conditions. The assumption of spherically symmetric profiles for the laser is therefore deemed valid, and it is a technique typically used by post-process CBET codes.

MAYBE?? Mention how ray noise means that we can't use direct deposition. Therefore use Pdep from field estimate, which is much cleaner.

Talk about how CBET enhances angular non-uniformity. Show modal decomposition.

1.7 Future Model Extensions

Say that there is even more laser/ CBET physics that is interesting and can be implemented within the raytracing framework. Some are straightforward to implement, while others more difficult and computationally expensive.

1.7.1 Langdon Effect on Abosprtion

Describe Langdon from a kinetic perspective and why it reduces absorption. Describe how you can fit it and include as a modification to ray tracing absorption if you have the field/ intensity. Describe the magnitude of the effect for ICF like conditions. Describe breifly how it would be implemented, say it would not be difficult.

1.7.2 Langdon Effect on CBET

Describe what this is. Say that it is important for high overlapping intensities, eg hohlraum LEH. Say that it is thought to stabilise the CBET interaction in indirect drive configurations and remove the need for artificial clamps. Describe breifly how it would be implemented, say it would not be difficult.

1.7.3 Polarised CBET

Describe how ion accoustic waves are driven by beat between electric fields from light and therefore is polarisation dependent. Say how on OMEGA, RPP smoothing means that each beam is split into 2 sub-beams with linear polarisation. Say that these do not have a symmetry to the configuration about the sphere. Say that this leads to mode-1 on OMEGA. Say that you can track polarisation of rays and trace these sub-beams independently. Would make it more expensive, but definitely feasible.

1.7.4 Bandwidth for CBET Mitigation Studies

Describe how bandwidth should reduce LPI growth rates. Understanding the desired bandwidth to mitigate CBET is a key consideration for design of future laser sysytems. Fields can be modified to include discrete wavelengths to model bandwidth.

1.7.5 Additional LPIs

Could look at TPD, SBS and SRS. In theory not a difficult problem to do backscatter, but side-SRS is difficult, because additional rays would need to be launched. This could make the model more useful to indirect-drive experiments and design of ignition scale direct-drive facilities, where SRS is thought to be important energetically due to long scale lengths.

1.8 Conclusions

Say that the chapter has described the validity and implementation of SOLAS and validated it. Culminated in demonstrating that the model can reproduce post-shot simulations of an OMEGA shot from the LILAC code which includes a CBET model. This demonstrates that the CHIMERA code now has a predictive capability for OMEGA scale direct drive experiments, as no free parameter tuning was required.

Appendices

A Numerics Appendices

Bibliography

[1] P. Tzeferacos, A. Rigby, A. F. A. Bott, A. R. Bell, R. Bingham, A. Casner, F. Cattaneo, E. M. Churazov, J. Emig, F. Fiuza, C. B. Forest, J. Foster, C. Graziani, J. Katz, M. Koenig, C.-K. Li, J. Meinecke, R. Petrasso, H.-S. Park, B. A. Remington, J. S. Ross, D. Ryu, D. Ryutov, T. G. White, B. Reville, F. Miniati, A. A. Schekochihin, D. Q. Lamb, D. H. Froula, and G. Gregori. Laboratory evidence of dynamo amplification of magnetic fields in a turbulent plasma. Nature Communications, 9 (1):591, February 2018. ISSN 2041-1723. doi: 10.1038/s41467-018-02953-2. URL `https://www.nature.com/articles/s41467-018-02953-2`. 6

[2] F. Fiuza, G. F. Swadling, A. Grassi, H. G. Rinderknecht, D. P. Higginson, D. D. Ryutov, C. Bruulsema, R. P. Drake, S. Funk, S. Glenzer, G. Gregori, C. K. Li, B. B. Pollock, B. A. Remington, J. S. Ross, W. Rozmus, Y. Sakawa, A. Spitkovsky, S. Wilks, and H.-S. Park. Electron acceleration in laboratory-produced turbulent collisionless shocks. Nature Physics, 16(9):916–920, September 2020. ISSN 1745-2481. doi: 10.1038/s41567-020-0919-4. URL `https://www.nature.com/articles/s41567-020-0919-4`. Publisher: Nature Publishing Group.

[3] Jena Meinecke, Petros Tzeferacos, James S. Ross, Archie F. A. Bott, Scott Feister, Hye-Sook Park, Anthony R. Bell, Roger Blandford, Richard L. Berger, Robert Bingham, Alexis Casner, Laura E. Chen, John Foster, Dustin H. Froula, Clement Goyon, Daniel Kalantar, Michel Koenig, Brandon Lahmann, Chikang Li, Yingchao Lu, Charlotte A. J. Palmer, Richard D. Petrasso, Hannah Poole, Bruce Remington, Brian Reville, Adam Reyes, Alexandra Rigby, Dongsu Ryu, George Swadling, Alex Zylstra, Francesco Miniati, Subir Sarkar, Alexander A. Schekochihin, Donald Q. Lamb, and Gianluca Gregori. Strong suppression of heat conduction in a laboratory replica of galaxy-cluster turbulent plasmas. Science Advances, 8 (10):eabj6799, March 2022. ISSN 2375-2548. doi: 10.1126/sciadv.abj6799. URL `https://www.science.org/doi/10.1126/sciadv.abj6799`. 6

[4] Andrea L. Kritcher, Damian C. Swift, Tilo Döppner, Benjamin Bachmann, Lorin X. Benedict, Gilbert W. Collins, Jonathan L. DuBois, Fred Elsner, Gilles Fontaine, Jim A. Gaffney, Sebastien Hamel, Amy Lazicki, Walter R. Johnson, Natalie Kostinski, Dominik Kraus, Michael J. MacDonald, Brian Maddox, Madison E. Martin, Paul Neumayer, Abbas Nikroo, Joseph Nilsen, Bruce A. Remington, Didier Saumon, Phillip A. Sterne, Wendi Sweet, Alfredo A. Correa, Heather D. Whitley, Roger W. Falcone, and Siegfried H. Glenzer. A measurement of the equa-

tion of state of carbon envelopes of white dwarfs. Nature, 584(7819):51–54, August 2020. ISSN 0028-0836, 1476-4687. doi: 10.1038/s41586-020-2535-y. URL `https://www.nature.com/articles/s41586-020-2535-y`. 6

[5] R. F. Smith, J. H. Eggert, R. Jeanloz, T. S. Duffy, D. G. Braun, J. R. Patterson, R. E. Rudd, J. Biener, A. E. Lazicki, A. V. Hamza, J. Wang, T. Braun, L. X. Benedict, P. M. Celliers, and G. W. Collins. Ramp compression of diamond to five terapascals. Nature, 511(7509):330–333, July 2014. ISSN 1476-4687. doi: 10.1038/nature13526. URL `https://www.nature.com/articles/nature13526`. Publisher: Nature Publishing Group. 6

[6] A. B. Zylstra, O. A. Hurricane, D. A. Callahan, A. L. Kritcher, J. E. Ralph, H. F. Robey, J. S. Ross, C. V. Young, K. L. Baker, D. T. Casey, T. Döppner, L. Divol, M. Hohenberger, S. Le Pape, A. Pak, P. K. Patel, R. Tommasini, S. J. Ali, P. A. Amendt, L. J. Atherton, B. Bachmann, D. Bailey, L. R. Benedetti, L. Berzak Hopkins, R. Betti, S. D. Bhandarkar, J. Biener, R. M. Bionta, N. W. Birge, E. J. Bond, D. K. Bradley, T. Braun, T. M. Briggs, M. W. Bruhn, P. M. Celliers, B. Chang, T. Chapman, H. Chen, C. Choate, A. R. Christopherson, D. S. Clark, J. W. Crippen, E. L. Dewald, T. R. Dittrich, M. J. Edwards, W. A. Farmer, J. E. Field, D. Fittinghoff, J. Frenje, J. Gaffney, M. Gatu Johnson, S. H. Glenzer, G. P. Grim, S. Haan, K. D. Hahn, G. N. Hall, B. A. Hammel, J. Harte, E. Hartouni, J. E. Heebner, V. J. Hernandez, H. Herrmann, M. C. Herrmann, D. E. Hinkel, D. D. Ho, J. P. Holder, W. W. Hsing, H. Huang, K. D. Humbird, N. Izumi, L. C. Jarrott, J. Jeet, O. Jones, G. D. Kerbel, S. M. Kerr, S. F. Khan, J. Kilkenny, Y. Kim, H. Geppert Kleinrath, V. Geppert Kleinrath, C. Kong, J. M. Koning, J. J. Kroll, M. K. G. Kruse, B. Kustowski, O. L. Landen, S. Langer, D. Larson, N. C. Lemos, J. D. Lindl, T. Ma, M. J. MacDonald, B. J. MacGowan, A. J. Mackinnon, S. A. MacLaren, A. G. MacPhee, M. M. Marinak, D. A. Mariscal, E. V. Marley, L. Masse, K. Meaney, N. B. Meezan, P. A. Michel, M. Millot, J. L. Milovich, J. D. Moody, A. S. Moore, J. W. Morton, T. Murphy, K. Newman, J.-M. G. Di Nicola, A. Nikroo, R. Nora, M. V. Patel, L. J. Pelz, J. L. Peterson, Y. Ping, B. B. Pollock, M. Ratledge, N. G. Rice, H. Rinderknecht, M. Rosen, M. S. Rubery, J. D. Salmonson, J. Sater, S. Schiaffino, D. J. Schlossberg, M. B. Schneider, C. R. Schroeder, H. A. Scott, S. M. Sepke, K. Sequoia, M. W. Sherlock, S. Shin, V. A. Smalyuk, B. K. Spears, P. T. Springer, M. Stadermann, S. Stoupin, D. J. Strozzi, L. J. Suter, C. A. Thomas, R. P. J. Town, E. R. Tubman, C. Trosseille, P. L. Volegov, C. R. Weber, K. Widmann, C. Wild, C. H. Wilde, B. M. Van Wonterghem, D. T. Woods, B. N. Woodworth, M. Yamaguchi, S. T. Yang, and G. B. Zimmerman. Burning plasma achieved in inertial fusion. Nature, 601 (7894):542–548, January 2022. ISSN 1476-4687. doi: 10.1038/s41586-021-04281-w. URL `https://www.nature.com/articles/s41586-021-04281-w`. Publisher: Nature Publishing Group. 6

[7] Stephen A. Slutz and Roger A. Vesey. High-Gain Magnetized Inertial Fusion. Physical Review Letters, 108(2):025003, January 2012. ISSN 0031-9007, 1079-7114. doi: 10.1103/PhysRevLett.108.025003. URL `https://link.aps.org/doi/10.1103/PhysRevLett.108.025003`.

[8] C. A. Williams, R. Betti, V. Gopalaswamy, J. P. Knauer, C. J. Forrest, A. Lees, R. Ejaz, P. S. Farmakis, D. Cao, P. B. Radha, K. S. Anderson, S. P. Regan, V. Yu Glebov, R. C. Shah, C. Stoeckl, S. Ivancic, K. Churnetski, R. T. Janezic, C. Fella, M. J. Rosenberg, M. J. Bonino, D. R. Harding, W. T. Shmayda, J. Carroll-Nellenback, S. X. Hu, R. Epstein, T. J. B. Collins, C. A. Thomas, I. V. Igumenshchev, V. N. Goncharov, W. Theobald, K. M. Woo, J. A. Marozas, K. A. Bauer, S. Sampat, L. J. Waxer, D. Turnbull, P. V. Heuer, H. McClow, L. Ceurvorst, W. Scullin, D. H. Edgell, M. Koch, D. Bredesen, M. Gatu Johnson, J. A. Frenje, R. D. Petrasso, C. Shuldberg, M. Farrell, J. Murray, D. Guzman, B. Serrato, S. F. B. Morse, M. Labuzeta, C. Deeney, and E. M. Campbell. Demonstration of hot-spot fuel gain exceeding unity in direct-drive inertial confinement fusion implosions. Nature Physics, 20(5):758–764, May 2024. ISSN 1745-2481. doi: 10.1038/s41567-023-02363-2. URL `https://www.nature.com/articles/s41567-023-02363-2`. Publisher: Nature Publishing Group. 6

[9] K. L. Nguyen, L. Yin, B. J. Albright, A. M. Hansen, D. H. Froula, D. Turnbull, R. K. Follett, and J. P. Palastro. Cross-beam energy transfer saturation by ion trapping-induced detuning. Physics of Plasmas, 28(8):082705, August 2021. ISSN 1070-664X, 1089-7674. doi: 10.1063/5.0054008. URL `https://pubs.aip.org/aip/pop/article/106807`. 6, 10

[10] J. F. Myatt, R. K. Follett, J. G. Shaw, D. H. Edgell, D. H. Froula, I. V. Igumenshchev, and V. N. Goncharov. A wave-based model for cross-beam energy transfer in direct-drive inertial confinement fusion. Physics of Plasmas, 24(5):056308, April 2017. ISSN 1070-664X. doi: 10.1063/1.4982059. URL `https://doi.org/10.1063/1.4982059`. 6, 10

[11] Andrew J. Schmitt and Stephen P. Obenschain. The importance of laser wavelength for driving inertial confinement fusion targets. I. Basic physics. Physics of Plasmas, 30(1):012701, January 2023. ISSN 1070-664X, 1089-7674. doi: 10.1063/5.0118080. URL `https://pubs.aip.org/pop/article/30/1/012701/2867678/The-importance-of-laser-wavelength-for-driving`. 7

[12] Andrew J. Schmitt and Stephen P. Obenschain. The importance of laser wavelength for driving inertial confinement fusion targets. II. Target design. Physics of Plasmas, 30(1):012702, January 2023. ISSN 1070-664X. doi: 10.1063/5.0118093. URL `https://doi.org/10.1063/5.0118093`. 7

[13] J Huba, D. NRL Plasma Formulary. Technical Report NRL/PU/6790–13-589, Washington, DC, 2013. 7

[14] Tudor Wyatt Johnston and John M. Dawson. Correct values for high-frequency power absorption by inverse bremsstrahlung in plasmas. Physics of Fluids, 16: 722–722, May 1973. ISSN 0899-82131070-6631. doi: 10.1063/1.1694419. URL https://ui.adsabs.harvard.edu/abs/1973PhFl...16..722J. Publisher: AIP ADS Bibcode: 1973PhFl...16..722J. 7

[15] A. Colaïtis, I. Igumenshchev, J. Mathiaud, and V. Goncharov. Inverse ray tracing on icosahedral tetrahedron grids for non-linear laser plasma interaction coupled to 3D radiation hydrodynamics. Journal of Computational Physics, 443:110537, October 2021. ISSN 0021-9991. doi: 10.1016/j.jcp.2021.110537. URL https://www.sciencedirect.com/science/article/pii/S0021999121004320. 7, 8

[16] C. J. Randall, James R. Albritton, and J. J. Thomson. Theory and simulation of stimulated Brillouin scatter excited by nonabsorbed light in laser fusion systems. The Physics of Fluids, 24(8):1474–1484, August 1981. ISSN 0031-9171. doi: 10.1063/1.863551. URL https://doi.org/10.1063/1.863551. 7

[17] A. Colaïtis, G. Duchateau, P. Nicolaï, and V. Tikhonchuk. Towards modeling of nonlinear laser-plasma interactions with hydrocodes: The thick-ray approach. Physical Review E, 89(3):033101, March 2014. doi: 10.1103/PhysRevE.89.033101. URL https://link.aps.org/doi/10.1103/PhysRevE.89.033101. Publisher: American Physical Society. 7, 9

[18] R. W. Paddock, H. Martin, R. T. Ruskov, R. H. H. Scott, W. Garbett, B. M. Haines, A. B. Zylstra, R. Aboushelbaya, M. W. Mayr, B. T. Spiers, R. H. W. Wang, and P. A. Norreys. One-dimensional hydrodynamic simulations of low convergence ratio direct-drive inertial confinement fusion implosions. Philosophical Transactions of the Royal Society A: Mathematical, Physical and Engineering Sciences, 379(2189): 20200224, January 2021. ISSN 1364-503X, 1471-2962. doi: 10.1098/rsta.2020.0224. URL https://royalsocietypublishing.org/doi/10.1098/rsta.2020.0224. 7

[19] A. Colaïtis, J. P. Palastro, R. K. Follett, I. V. Igumenschev, and V. Goncharov. Real and complex valued geometrical optics inverse ray-tracing for inline field calculations. Physics of Plasmas, 26(3):032301, March 2019. ISSN 1070-664X, 1089-7674. doi: 10.1063/1.5082951. URL https://pubs.aip.org/pop/article/26/3/032301/699557/Real-and-complex-valued-geometrical-optics-inverse. 8

[20] A. Colaïtis, R. K. Follett, J. P. Palastro, I. Igumenschev, and V. Goncharov. Adaptive inverse ray-tracing for accurate and efficient modeling of cross beam energy transfer in hydrodynamics simulations. Physics of Plasmas, 26(7):072706, July 2019. ISSN 1070-664X, 1089-7674. doi: 10.1063/1.5108777. URL https://pubs.aip.org/pop/article/26/7/072706/1060189/Adaptive-inverse-ray-tracing-for-accurate-and. 8

[21] D. J. Strozzi, D. S. Bailey, P. Michel, L. Divol, S. M. Sepke, G. D. Kerbel, C. A. Thomas, J. E. Ralph, J. D. Moody, and M. B. Schneider. Interplay of Laser-Plasma

Interactions and Inertial Fusion Hydrodynamics. Physical Review Letters, 118(2): 025002, January 2017. ISSN 0031-9007, 1079-7114. doi: 10.1103/PhysRevLett.118.025002. URL https://link.aps.org/doi/10.1103/PhysRevLett.118.025002. 8

[22] S. Liberatore, P. Gauthier, J. L. Willien, P. E. Masson-Laborde, F. Philippe, O. Poujade, E. Alozy, R. Botrel, G. Boutoux, J. Bray, T. Caillaud, C. Chicanne, C. Chollet, A. Debayle, S. Depierreux, W. Duchastenier, M. Ferri, O. Henry, P. Hoch, S. Laffite, O. Landoas, L. Le-Deroff, E. Lefebvre, G. Legay, I. Marmajou, C. Meyer, K. Molina, O. Morice, E. Peche, P. Prunet, R. Riquier, R. Rosch, V. Tassin, X. Vaisseau, and B. Villette. First indirect drive inertial confinement fusion campaign at Laser Megajoule. Physics of Plasmas, 30(12):122707, December 2023. ISSN 1070-664X, 1089-7674. doi: 10.1063/5.0176446. URL https://pubs.aip.org/pop/article/30/12/122707/2930727/First-indirect-drive-inertial-confinement-fusion. 8

[23] J. A. Marozas, M. Hohenberger, M. J. Rosenberg, D. Turnbull, T. J. B. Collins, P. B. Radha, P. W. McKenty, J. D. Zuegel, F. J. Marshall, S. P. Regan, T. C. Sangster, W. Seka, E. M. Campbell, V. N. Goncharov, M. W. Bowers, J.-M. G. Di Nicola, G. Erbert, B. J. MacGowan, L. J. Pelz, J. Moody, and S. T. Yang. Wavelength-detuning cross-beam energy transfer mitigation scheme for direct drive: Modeling and evidence from National Ignition Facility implosions. Physics of Plasmas, 25(5):056314, May 2018. ISSN 1070-664X, 1089-7674. doi: 10.1063/1.5022181. URL https://pubs.aip.org/pop/article/25/5/056314/1061159/Wavelength-detuning-cross-beam-energy-transfer. 8

[24] A. Debayle, C. Ruyer, O. Morice, P.-E. Masson-Laborde, P. Loiseau, and D. Benisti. A unified modeling of wave mixing processes with the ray tracing method. Physics of Plasmas, 26(9):092705, September 2019. ISSN 1070-664X, 1089-7674. doi: 10.1063/1.5110247. URL https://pubs.aip.org/pop/article/26/9/092705/263616/A-unified-modeling-of-wave-mixing-processes-with. 9

[25] A. Colaïtis, S. Hüller, D. Pesme, G. Duchateau, and V. T. Tikhonchuk. Crossed beam energy transfer: Assessment of the paraxial complex geometrical optics approach versus a time-dependent paraxial method to describe experimental results. Physics of Plasmas, 23(3):032118, March 2016. ISSN 1070-664X, 1089-7674. doi: 10.1063/1.4944496. URL https://pubs.aip.org/pop/article/23/3/032118/1016773/Crossed-beam-energy-transfer-Assessment-of-the. 9

[26] A. Colaïtis, G. Duchateau, X. Ribeyre, and V. Tikhonchuk. Modeling of the cross-beam energy transfer with realistic inertial-confinement-fusion beams in a large-scale hydrocode. Physical Review E, 91(1):013102, January 2015. ISSN 1539-3755, 1550-2376. doi: 10.1103/PhysRevE.91.013102. URL https://link.aps.org/doi/10.1103/PhysRevE.91.013102. 10

[27] D. H. Edgell, R. K. Follett, I. V. Igumenshchev, J. F. Myatt, J. G. Shaw, and D. H. Froula. Mitigation of cross-beam energy transfer in symmetric implosions

on OMEGA using wavelength detuning. Physics of Plasmas, 24(6):062706, June 2017. ISSN 1070-664X, 1089-7674. doi: 10.1063/1.4985315. URL https://pubs.aip.org/aip/pop/article/108749. 10

[28] R. K. Follett, J. G. Shaw, J. F. Myatt, V. N. Goncharov, D. H. Edgell, D. H. Froula, and J. P. Palastro. Ray-based modeling of cross-beam energy transfer at caustics. Physical Review E, 98(4):043202, October 2018. ISSN 2470-0045, 2470-0053. doi: 10.1103/PhysRevE.98.043202. URL https://link.aps.org/doi/10.1103/PhysRevE.98.043202. 10

[29] R. K. Follett, A. Colaïtis, D. Turnbull, D. H. Froula, and J. P. Palastro. Validation of ray-based cross-beam energy transfer models. Physics of Plasmas, 29(11):113902, November 2022. ISSN 1070-664X, 1089-7674. doi: 10.1063/5.0123462. URL https://pubs.aip.org/pop/article/29/11/113902/2844248/Validation-of-ray-based-cross-beam-energy-transfer. 10

[30] Jason F. Myatt, John G. Shaw, Russell K. Follett, Dana H. Edgell, Dustin H. Froula, John P. Palastro, and Valeri N. Goncharov. LPSE: A 3-D wave-based model of cross-beam energy transfer in laser-irradiated plasmas. Journal of Computational Physics, 399:108916, December 2019. ISSN 00219991. doi: 10.1016/j.jcp.2019.108916. URL https://linkinghub.elsevier.com/retrieve/pii/S0021999119306217. 10

[31] R. K. Follett, J. G. Shaw, J. F. Myatt, H. Wen, D. H. Froula, and J. P. Palastro. Thresholds of absolute two-plasmon-decay and stimulated Raman scattering instabilities driven by multiple broadband lasers. Physics of Plasmas, 28(3):032103, March 2021. ISSN 1070-664X, 1089-7674. doi: 10.1063/5.0037869. URL https://pubs.aip.org/pop/article/28/3/032103/835482/Thresholds-of-absolute-two-plasmon-decay-and. 10

[32] L. J. Perkins, R. Betti, K. N. LaFortune, and W. H. Williams. Shock Ignition: A New Approach to High Gain Inertial Confinement Fusion on the National Ignition Facility. Physical Review Letters, 103(4):045004, July 2009. ISSN 0031-9007, 1079-7114. doi: 10.1103/PhysRevLett.103.045004. URL https://link.aps.org/doi/10.1103/PhysRevLett.103.045004. 10

[33] A. G. Seaton, L. Yin, R. K. Follett, B. J. Albright, and A. Le. Cross-beam energy transfer in direct-drive ICF. II. Theory and simulation of mitigation through increased laser bandwidth. Physics of Plasmas, 29(4):042707, April 2022. ISSN 1070-664X. doi: 10.1063/5.0078801. URL https://doi.org/10.1063/5.0078801. 11

[34] A. G. Seaton, L. Yin, R. K. Follett, B. J. Albright, and A. Le. Cross-beam energy transfer in direct-drive ICF. I. Nonlinear and kinetic effects. Physics of Plasmas, 29(4):042706, April 2022. ISSN 1070-664X. doi: 10.1063/5.0078800. URL https://doi.org/10.1063/5.0078800. 11

Permissions